Assessment of Braking Dynamics of Passenger Cars Operating in the Mekong Delta Region of Vietnam

Phat Khau Tan and Danh Nguyen Thanh *

Faculty of Automotive Engineering Technology, Vinh Long University of Technology Education, Vinh Long, Vietnam
Email: Phatkt@vlute.edu.vn (P.K.T.); Danhnt@vlute.edu.vn (D.N.T.)
*Corresponding author

***Abstract*—This study presents an experimental investigation into the braking dynamics of automobiles operating under typical road conditions in the Mekong Delta region, using a Kistler dynamic testing device. The primary objective of the study is to evaluate braking efficiency and capture key dynamic parameters during braking maneuvers with high measurement accuracy. The Kistler dynamic testing system was selected due to its ability to provide reliable, high-resolution data, allowing a precise assessment of braking performance under controlled experimental conditions. Braking tests were conducted at a constant initial vehicle speed of 80 km/h on road surfaces with friction coefficients of 0.5, 0.7, and 0.8. During each braking event, critical dynamic variables were recorded, including wheel slip ratio, vehicle speed variation during braking, vertical reaction forces at both the front and rear wheels, longitudinal body pitch angle, and braking distance. These parameters provide comprehensive insight into the braking behavior and stability of the vehicle under different friction conditions. Based on the experimental results, key input parameters were identified for the development of a future theoretical and numerical simulation model of vehicle braking dynamics. The close agreement between measured data and expected physical behavior demonstrates the reliability of the experimental setup and confirms the effectiveness of the Kistler dynamic testing device in capturing braking performance characteristics. The findings establish a solid experimental foundation for subsequent modeling and simulation studies aimed at improving braking efficiency and safety of automobiles operating in the Mekong Delta.**

***Keywords*—braking dynamic, dynamics experiment, braking efficiency, deceleration**

I. Introduction

Traffic safety remains a critical issue in Vietnam, where passenger cars frequently experience stability loss during braking, leading to serious traffic accidents. This situation is largely attributed to unfavorable road conditions, including uneven pavement surfaces, degraded infrastructure, and limited maintenance, combined with a tropical climate characterized by frequent rainfall throughout the year [1]. Wet and low-adhesion road surfaces significantly reduce tire-road friction, thereby increasing braking distance and the likelihood of wheel slip and vehicle instability [2]. Under such conditions, accurately understanding the braking dynamics of passenger cars becomes essential for improving vehicle safety and developing effective braking control strategies.

The braking process of a vehicle is a complex dynamic phenomenon influenced by multiple factors, including vehicle speed, tire-road adhesion, load transfer between axles, and suspension characteristics. Variations in road surface conditions can significantly alter the distribution of vertical reaction forces and wheel slip behavior, directly affecting braking efficiency and directional stability [3]. In response to these challenges, the author previously developed a dynamic model and a system of governing equations describing the braking dynamics of passenger cars [4]. This theoretical framework provides a basis for analyzing the interaction between braking forces, vehicle motion, and tire-road contact conditions.

However, accurate simulation of braking dynamics requires reliable input parameters that reflect real operating conditions. Therefore, an experimental model was developed to investigate the influence of road surface characteristics on braking performance. Braking dynamics experiments were conducted using a Kistler dynamic testing device, which allows high-precision measurement of key variables during braking maneuvers [5]. The experimental setup enabled direct measurement of braking acceleration, vertical reaction forces at the wheels, braking distance, and slip coefficient under controlled conditions.

To ensure safety and repeatability, experiments were performed with a passenger car traveling at an initial speed of 80 km/h on road surfaces with low and medium adhesion coefficients of 0.5, 0.7, and 0.8, respectively. Based on the experimental results, braking efficiency was evaluated for each operating condition. The obtained data provide a reliable foundation for subsequent simulation studies and contribute to a more accurate assessment of vehicle braking performance under adverse road

Manuscript received March 13, 2026; revised April 22, 2026; accepted June 2, 2026; published September 8, 2026.

doi: 10.18178/ijmerr.15.5.433-444

conditions, supporting future research in vehicle dynamics modeling and traffic.

The novelty of this study does not lie solely in conducting braking experiments under varying friction conditions, which have indeed been addressed in prior literature, but rather in the context, structure, and depth of the experimental investigation. Specifically, this work targets real-world operating conditions in the Mekong Delta, where road surfaces are highly heterogeneous due to persistent moisture, low-quality pavement, and seasonal degradation—conditions that are not adequately represented in conventional experimental studies conducted under controlled or standardized environments.

The creation of a uniform experimental framework that examines various adhesion levels under the same vehicle and testing conditions is a significant contribution of this work. This method makes it possible to compare brake dynamics directly and methodically, removing discrepancies that are sometimes present in research that depends on different datasets or simulation assumptions. Specifically, a coupled interpretation of braking behavior that goes beyond solitary parameter evaluation is provided by the simultaneous measurement and analysis of slip ratio evolution, vertical load transfer, braking force variation, and deceleration.

Moreover, the results offer experimentally grounded insights into the mechanisms leading to rear-wheel instability and rapid transition to full slip under medium and low adhesion conditions. These findings contribute to a more detailed understanding of braking-induced instability in practical driving environments and provide a reliable empirical basis for the calibration and validation of future dynamic models and control strategies.

In recent years, numerous studies on vehicle braking dynamics have relied heavily on numerical simulations to evaluate system performance under various operating conditions. However, such approaches typically depend on simplified assumptions regarding tire-road interaction, suspension characteristics, and road surface excitation, which may limit their ability to accurately capture real-world dynamic behavior, particularly under irregular road conditions.

To address these limitations, this study adopts an experimentally driven approach, in which high-resolution measurements are employed to directly characterize the dynamic response of the vehicle during braking. A dynamic model is developed to describe the fundamental relationships between braking force, vertical load transfer, and road-induced excitation. Rather than being used for numerical simulation, the proposed model serves as a theoretical framework to interpret the experimental observations and to provide physical insight into the measured phenomena.

By prioritizing experimental validation over simulation-based prediction, this work aims to provide more realistic and practically relevant findings, especially for conditions where modeling uncertainties remain significant.

II. Overview of Related Research Studies

The evaluation of braking dynamics for passenger vehicles has transitioned from classical mechanical modeling to a multidisciplinary approach that integrates reliability-oriented diagnosis and real-time safety assessment. In geologically complex regions like the Mekong Delta of Vietnam, braking performance is not merely a function of hardware integrity but is dictated by extremely low-adhesion conditions resulting from high humidity, frequent precipitation, and degraded road infrastructure.

In the field of automotive safety, experimental studies by Zulhilmi *et al.* [6] investigated the specific effects of emergency braking without an anti-lock braking system on vehicle dynamic behavior, which was further expanded by their subsequent analysis of vehicle responses during emergency braking at varying initial speeds [7]. To address these braking instabilities, advanced control mechanisms have been continuously developed; for instance, Eze *et al.* [8] proposed a novel model reference adaptive control-based PID controller at the wheel slip equilibrium point to optimize ABS performance, while Haris *et al.* [9] implemented a self-tuning PID control scheme tailored for electronic wedge brakes, building upon foundational methodologies such as the sliding-mode PWM control for hydraulic ABS developed by Wu and Shih [10].

Beyond standard passenger vehicles, active braking principles have been adapted for alternative mobility platforms, as shown by Heerwan *et al.* [11] in their evaluation of a plugging braking system for electric wheelchair hill descent control. In the context of Vietnamese transportation, ensuring such safety standards is strictly governed by the national technical regulation QCVN 09:2015/BGTVT [12].

Aligning with these regulatory frameworks, localized dynamic challenges have been explored by Le *et al.* [13] through a nonlinear dynamic analysis of the interaction between 5-axle heavy trucks and road surfaces. To further enhance global vehicle stability under complex conditions, Soltani *et al.* [14] developed an integrated control strategy combining both braking and steering systems based on optimal wheel slip estimation. Ultimately, these diverse experimental and control approaches contribute to the comprehensive theoretical and applied framework of vehicle dynamics synthesized by Jazar [15].

Despite these advancements, there is a clear literature gap regarding the localized application of these high-level diagnostic principles to passenger cars operating in the specific conditions of the Mekong Delta. This study fills this gap by establishing a methodological chain from field-collected experimental data to condition-based safety assessment, utilizing the principles of imbalanced-condition identification to ensure a robust evaluation of braking dynamics under complex operating environments.

III. Building A Car Dynamics Model

The longitudinal and lateral tire forces, represented by the symbols F_{xij} and F_{yij}, respectively, interact to control a vehicle's motion in the road plane, as shown in Fig. 1. The vertical reaction force F_{zij} at each wheel, which changes dynamically during braking as a result of load transfer effects, has a significant influence on these forces [16]. Variations in vertical load have a direct impact on tire-road adhesion, which in turn affects vehicle stability and braking effectiveness. Therefore, a thorough mathematical model that can capture the linked behavior of longitudinal, lateral, and vertical motions is necessary for an accurate description of vehicle braking dynamics.

Based on the structural separation method, the vehicle is decomposed into subsystems representing the sprung mass, unsprung masses, and wheel assemblies. The governing equations of motion are established using the Newton-Euler approach [17, 18], which allows systematic formulation of force and moment balance equations for each subsystem. This modeling strategy enables the representation of complex vehicle dynamics while maintaining computational efficiency and physical interpretability [19].

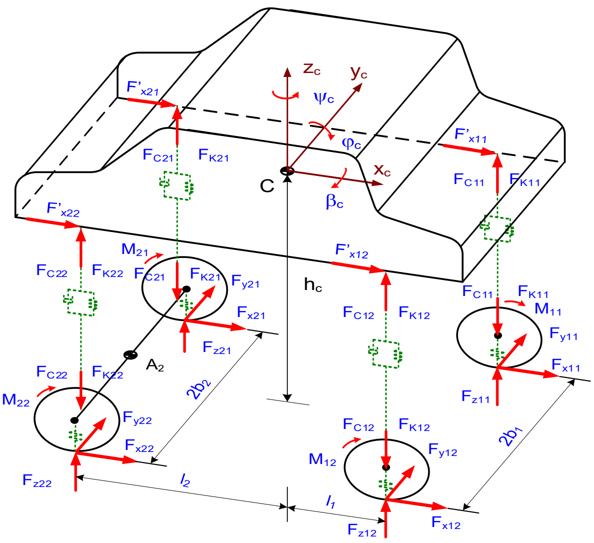

Fig. 1. Diagram of forces and moments acting on the car.

The translational motion of the vehicle's center of mass in the longitudinal (x_c) and lateral (y_c) directions as well as the yaw motion of the vehicle body around the vertical axis (z_c) are first described by the vehicle dynamics equations in the longitudinal plane (XOY). In order to assess directional stability during braking movements, these equations must take into account the impacts of braking forces, lateral tire forces, and yaw moments [20].

Second, the dynamics equations in the vertical plane (XOZ) are established to analyze longitudinal motion and pitching behavior of the vehicle body. This subsystem accounts for vertical load transfer between the front and rear axles during braking, enabling calculation of the vehicle's longitudinal oscillation (pitch) angle. Accurate modeling of this behavior is essential for determining the distribution of braking forces and vertical reactions at each axle [6, 10].

Third, the vertical motions of the left and right front axle wheels, axle 2's roll motion about the x_{A2} axis, and the sprung mass's lateral oscillation angle are all described by the dynamic equations in the horizontal plane (YOZ). These equations reflect asymmetric loading conditions and suspension responses that influence vehicle stability and comfort.

The rotational motion of each wheel is finally described by wheel dynamics equations, which connect tire forces, slip ratio, brake torque, and wheel angular speed. A thorough assessment of braking ability under various road adhesion situations is made possible by the combination of wheel dynamics with vehicle body motion. Together, this system of coupled equations provides a robust theoretical foundation for analyzing vehicle braking dynamics and serves as the basis for subsequent simulation and experimental validation.

Equation of motion along the x_c axis of the car [21]:

$$\begin{gathered}(m+m_1+m_2)(\ddot{x}_c+\dot{\psi}_c\dot{y}_c)=F_{x11}\cos\delta_{11}\\+F_{x12}\cos\delta_{12}-F_{y11}\sin\delta_{11}-F_{y12}\sin\delta_{12}+F_{x21}+F_{x22}\end{gathered}\tag{1}$$

Equation of horizontal motion y_c of the car:

$$\begin{gathered}(m+m_1+m_2)(\ddot{y}_c+\dot{\psi}_c\dot{x}_c)=F_{x11}\sin\delta_{11}\\+F_{x12}\sin\delta_{12}+F_{y11}\cos\delta_{11}+F_{y12}\cos\delta_{12}+F_{y21}+F_{y22}\end{gathered}\tag{2}$$

Equation of rotational motion around the z_c axis of the car body:

$$\begin{gathered}J_{zc}\ddot{\psi}_c=(F_{x11}\sin\delta_{11}+F_{x12}\sin\delta_{12}+F_{y11}\cos\delta_{11}\\+F_{y12}\cos\delta_{12})l_1+(F_{x22}-F_{x21})b_2\\+(F_{x12}\cos\delta_{12}-F_{x11}\cos\delta_{11}+F_{y11}\sin\delta_{11}\\-F_{y12}\sin\delta_{12})b_1-(F_{y21}+F_{y22})l_2\end{gathered}\tag{3}$$

The differential equation describing the vertical oscillation of the center of gravity of the suspended mass is written as follows [22]:

$$\begin{gathered}M\ddot{z}=F_{C11}+F_{K11}+F_{C12}+F_{K12}\\+F_{C21}+F_{K21}+F_{C22}+F_{K22}\end{gathered}\tag{4}$$

$$\begin{gathered}J_{yc}\ddot{\varphi}_c=(F_{C11}+F_{K11}+F_{C12}+F_{K12})l_1\\-(F_{C21}+F_{K21}+F_{C22}+F_{K22})l_2+M_{1j}+M_{2j}\end{gathered}\tag{5}$$

Equation of horizontal oscillation around the x_c axis for a suspended mass:

$$\begin{gathered}J_{xc}\ddot{\beta}_c=(F_{C12}+F_{K12}-F_{C11}-F_{K11})w_1\\+(F_{C22}+F_{K22}-F_{C21}-F_{K21})w_2\end{gathered}\tag{6}$$

Equation of vertical motion of the left front axle wheel:

$$m_1\ddot{\xi}_{11}=-(F_{K11}+F_{C11})+F_{CL11}\tag{7}$$

Equation of vertical motion of the right front axle wheel:

$$m_2\ddot{\xi}_{12}=-(F_{K12}+F_{12})+F_{CL12}\tag{8}$$

The vertical equation of motion (z) of the rear axle [23]:

$$\begin{aligned} m_3\ddot{z}_A &= F_{CL21} + F_{KL21} + F_{CL22} + F_{KL22} \\ &-F_{C21} - F_{K21} - F_{C22} - F_{K22} \end{aligned} \tag{9}$$

Equation of lateral oscillation motion around axis x_{A2} of bridge 2:

$$\begin{aligned} J_{Ax}\ddot{\beta}_A &= (F_{C21} + F_{K21} - F_{C22} - F_{K22})w_2 + (F_{CL22} + F_{KL22} \\ &-F_{CL21} - F_{KL21})b_2 - F_{y21}(r_{21} + \xi_{A21}) - F_{y22}(r_{22} + \xi_{A22}) \end{aligned} \tag{10}$$

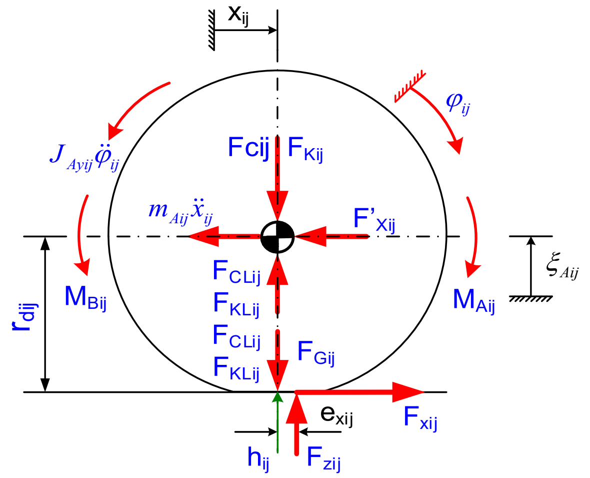

Fig. 2. Wheel dynamics diagram.

A wheel dynamics model is established in Fig. 2. Each of an automobile's two axles has one wheel on the left and one on the right. Each of an automobile's two axles has one wheel on the left and one on the right. For the four wheels in the longitudinal plane, we have the following equations [24]:

$$\begin{cases} J_{Ay11}\ddot{\varphi}_{11} = M_{A11} - M_{B11} - F_{z11}e_{x11} \\ J_{Ay12}\ddot{\varphi}_{12} = M_{A12} - M_{B12} - F_{z12}e_{x12} \\ J_{Ay21}\ddot{\varphi}_{21} = M_{A21} - M_{B21} - F_{z21}e_{x21} \\ J_{Ay22}\ddot{\varphi}_{22} = M_{A22} - M_{B22} - F_{z22}e_{x22} \end{cases} \tag{11}$$

A direct connection between the experimental data and the underlying vehicle dynamics theory is enabled by quantitatively analyzing the recorded phenomena using the theoretical models given in Eqs. (1)–(11).

IV. Experiment to Measure the Effectiveness of Car Brakes

To determine the normal reaction force from the road surface acting on the wheel, load cell force sensors are placed at the wheel, where there is direct contact between the wheel and the axle. A Kistler 8152C vehicle body acceleration sensor located in the center of the vehicle body provides signals to the computer. The speed sensors shown in Fig. 3 are installed on the wheels to measure the vehicle's speed; the computer uses these sensors as input parameters. Eq. (1) can be used to calculate the wheel slip coefficient based on the longitudinal acceleration, wheel velocity, and vehicle body velocity parameters while braking [25].

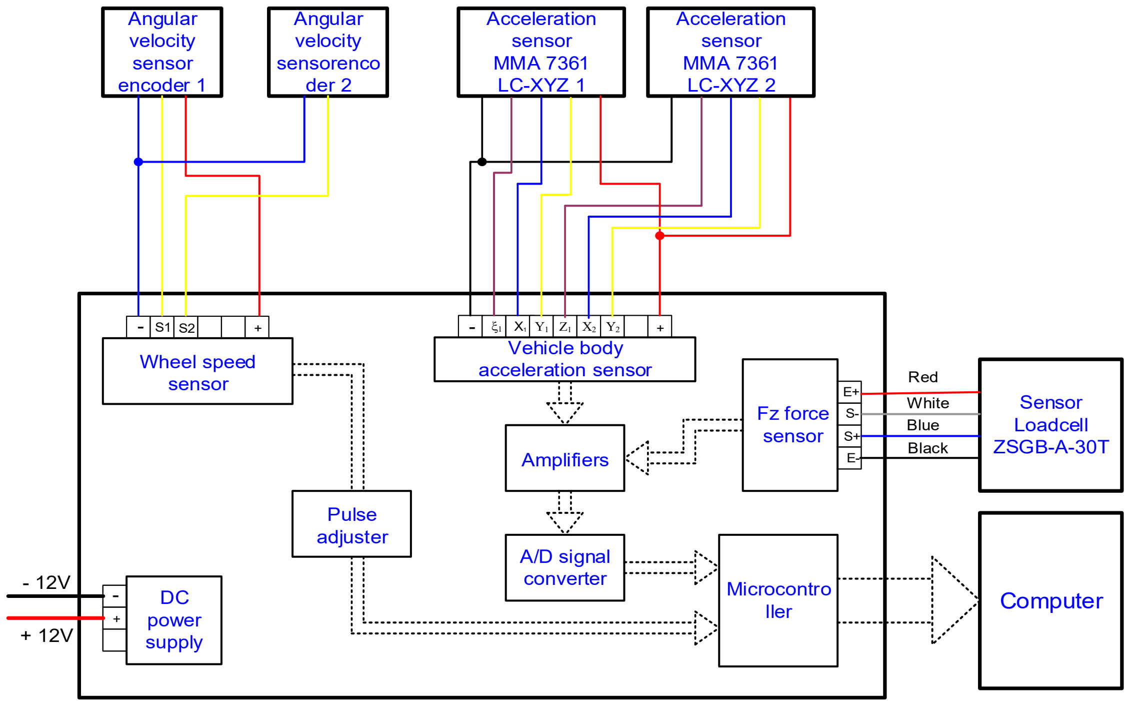

Fig. 3. Arrangement diagram of sensors measuring signals and processing measurement results.

Install the sensors according to the experimental layout diagram. Fig. 4 presents the experimental equipment, which is specialized dynamic testing equipment from Kistler, Germany. Fig. 5 presents Wheel velocity sensors, longitudinal vehicle velocity sensors during braking, and braking acceleration sensors, vertical reaction force sensors, and Fig. 6 presents other sensors that were installed directly on the vehicle to collect real-time data from the sensors throughout the experiment.

Fig. 4. Kisler dynamic laboratory apparatus.

Fig. 5. Kistler acceleration sensor 8152C.

Fig. 6. Sensor layout for real-time vehicle braking data acquisition.

Fig. 7 presents the computer receiving and processing signals sent from the sensors, then calculating and displaying the values of the vehicle's longitudinal velocity, wheel velocity, and deceleration during braking [26].

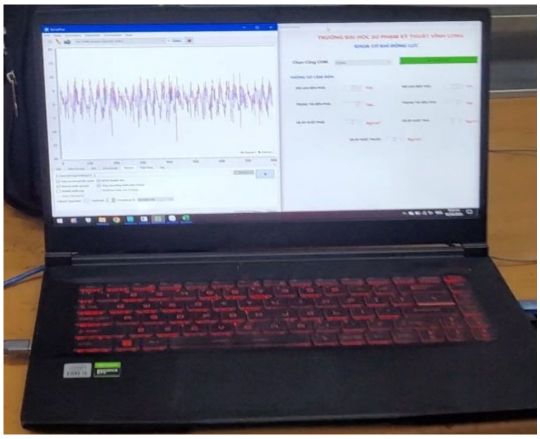

Fig. 7. Measured data from the sensors is sent to the computer, which processes it.

A. *Experimental Procedure*

To ensure the reliability and reproducibility of the experimental results, a structured and controlled testing procedure was implemented. The experiments were conducted using a passenger vehicle instrumented with a Kistler dynamic measurement system, enabling high-precision acquisition of braking-related parameters. During the experiments, the 11.00R20 radial tires on the experimental vehicle were kept at an inflation pressure of 750 kPa. To guarantee solid tire-road contact conditions, the tires' average tread depth was roughly 12 mm.

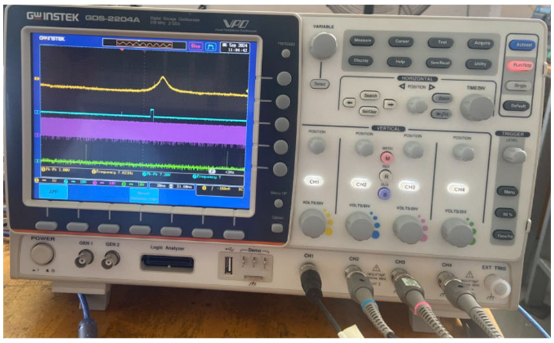

Fig. 8. Measure the output voltage using an oscilloscope.

Fig. 9. Circuit with capacitors CX, CY, CZ for data filtering.

To guarantee measurement accuracy, all sensors—including load cell force transducers, wheel speed sensors, and acceleration sensors—were calibrated in compliance with the manufacturer's specifications before testing. To record fleeting dynamic responses during braking, the data collection system was configured with a sufficiently high sampling rate.

To guarantee the precision and dependability of the recorded acceleration signals, the Kistler 8152C acceleration sensor was calibrated in accordance with the manufacturer's specifications prior to the experiments. Verifying sensor sensitivity, output stability, and measurement repeatability were the main goals of the calibration process. A conventional vibration calibration instrument, a stabilized power supply, and a high-precision oscilloscope for tracking the sensor output signals comprised the calibration setup. The acquired acceleration signal was evaluated during calibration by comparing the sensor's response with a reference excitation signal using an oscilloscope, as shown in Fig. 8.

The acceleration signals obtained were processed using a low-pass filter to reduce noise during vehicle vibration measurements, as shown in Fig. 9. According to ISO 2631-1, this method preserved the low-frequency vibration components associated with vehicle ride comfort while reducing high-frequency disturbances caused by undesired mechanical vibrations and electromagnetic interference. After three repetitions of each calibration condition, the mean values were utilized for further experimental analysis.

The test vehicle was operated under fully loaded conditions to reflect realistic driving scenarios. Key vehicle parameters, including total mass and load distribution, were kept constant throughout all experiments, as shown in Table I. The tires used in the tests were maintained at the manufacturer—recommended pressure to ensure consistency in tire-road interaction characteristics.

TABLE I. INPUT PARAMETERS OF THE SURVEY MODEL

TT	Parameter	Symbol	Value	Unit
1	Front and rear suspension stiffness	C_{11}, C_{12} C_{21}, C_{22}	175,000 326,000	N/m
2	Front and rear damping coefficients	K_{11}, K_{12} K_{21}, K_{22}	12,180 15,350	N.s/m
3	Front and rear tire radial stiffness	C_{L11}, $_{L12}$ C_{L21}, C_{L22}	350,000 652,000	N/m
4	The weight should not be suspended in front or behind.	m_{A1} m_{A2}	570 735	kg
5	Total weight of the fully loaded vehicle	M	1732	kg
6	The overall length of the vehicle	L_W	4.410	m
7	The overall width of the vehicle	B_W	1.700	m
8	The overall height of the vehicle	H_W	1.475	m
9	Wheelbase	L	2.500	m
10	Front wheel dynamic radius	r_1	0.4229	m
11	Rear wheel dynamic radius	r_2	0.4252	m
12	Moment of inertia of the vehicle body around the *x*-*y*-*z* axis.	J_x J_y J_z	4289 15,399 18,900	kgm^2
13	Moment of inertia of the front and rear axles around the longitudinal axis x	J_{Ax1} J_{Ax2}	285 335	kgm^2
14	Moment of inertia of the mass of the front wheels around the horizontal axis y	J_{Ay11}, $_{Ay12}$	10	kgm^2
15	Moment of inertia of the mass of the rear wheels around the horizontal axis y	J_{Ay21}, $_{Ay22}$	20	kgm^2

Road surfaces with varying adhesion conditions—corresponding to friction coefficients of 0.5, 0.7, and 0.8—were used for braking tests. Before braking, the car was first accelerated to a steady starting speed of 80 km/h for each test circumstance. To reduce random measurement errors, each experimental condition was performed three times, and the average data were chosen for further analysis. The driver initiated the braking procedure at the assigned test point by applying the brake system in a controlled and consistent manner.

Key dynamic characteristics, such as vehicle longitudinal velocity, wheel angular velocity, braking deceleration, vertical reaction forces at each axle, and slip ratio, were continually recorded by the measurement equipment throughout each braking event. These measurements were then processed to assess stability characteristics and braking performance.

To ensure repeatability, each test condition was repeated under identical operating conditions. The consistency of the recorded data across repeated trials confirmed the reliability of the experimental setup. Any anomalous data caused by external disturbances were excluded based on consistency checks. Overall, the experimental methodology was designed to provide a controlled yet representative assessment of braking dynamics, ensuring both measurement accuracy and the reproducibility of the obtained results.

The experiment was carried out with the car traveling at 80 km/h when fully loaded in order to confirm the car's braking efficiency. The driver kept the accelerator pedal depressed to keep the car moving continuously on the road surface, and the Kistler test apparatus recorded the results as soon as the driver began braking [27].

The vehicle body acceleration characteristics and the interior pressure of the pneumatic balloon were determined using the article's sensors and measuring instruments:

- Vertical acceleration sensors placed on the vehicle body at the contact points of the suspension system with the left and right sides of the vehicle body to measure the vertical acceleration of the vehicle body, shown as number 4 in Fig. 10.

- Vertical acceleration sensors placed on the axle at the contact points of the suspension system on the left and right sides to measure the vertical acceleration of the axle, shown as number 2 in Fig. 10.
- Longitudinal acceleration sensors placed on the vehicle body at the center of gravity to measure braking acceleration and vehicle body velocity during braking, shown as number 3 in Fig. 10.
- Angular velocity sensors for the wheels at the left and right front wheels, shown as number 1 in Fig. 10.

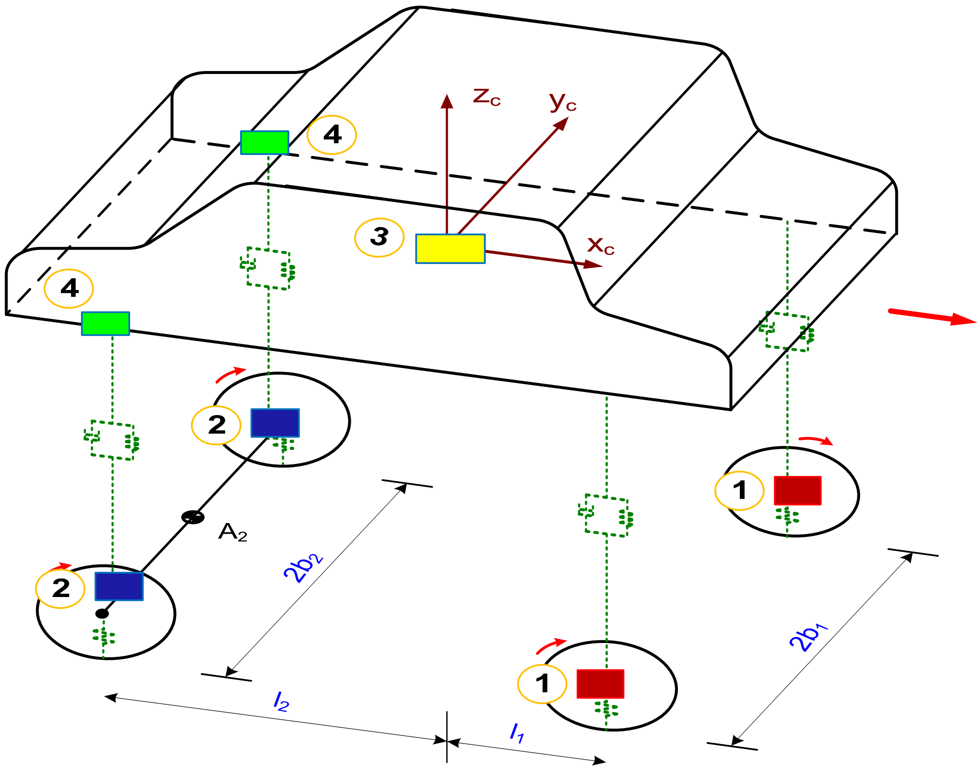

Fig. 10. Location of the experimental sensors.

Knowing the longitudinal and angular velocities of the wheels, we can determine the longitudinal slip coefficients of the wheels as follows:

$$s_{xij} = \begin{cases} -\frac{\dot{x}_{ij} - r_{dij}\dot{\varphi}_{xij}}{\dot{x}_{ij}} khi -1 \le s_{ij} \le 0 \\ \frac{r_{dij}\dot{\varphi}_{xij} - \dot{x}_{ij}}{r_{dij}\dot{\varphi}_{xij}} khi 0 < s_{ij} < 1 \end{cases} \tag{12}$$

In there: S_{xij} Wheel slip coefficient; $\dot{x}_{ij}$ The x-axis velocity of the car; $r_{dij}\dot{\varphi}_{xij}$ wheel angular velocity; $i = 1 \div 2$, $j = 1$ (Left), $j = 2$ (Right)

B. Survey Results

The longitudinal velocity of the car body during braking, the wheel speed during braking, the vertical reaction force from the road surface on the wheels on the bridge, and the coefficient of slip of the car when braking on a road with a low adhesion coefficient φ = 0.5, a medium adhesion coefficient φ = 0.7 and high adhesion coefficient φ = 0.8 were all determined by the experimental results.

According to the experimental findings of the "Magic Formula" in Hans Pacejka's book Tire and Vehicle Dynamics, there is a non-linear relationship between a tire's slip ratio and coefficient of friction (φ) [28]. This model demonstrated that the ideal braking force achieves its greatest value (S_{max}%) when the slip ratio varies between 15% and 20%, rather than when the wheel is fully locked (100% slip). This serves as the basic theoretical foundation for the programming and construction of active control systems like ABS found in contemporary cars.

TABLE II. EXPERIMENTAL RESULTS AND CRITERIA FOR SLIDING COEFFICIENTS

Sliding Coefficient	φ = 0.5 (%)	φ = 0.7 (%)	φ = 0.8 (%)	Slip Coefficient Standard
S_{11max}	5.5	3.5	2.2	10–15
S_{21max}	100 (0.6 s ≥ 5 s)	100 (0.8 s ≥ 5 s)	9.5	10–15

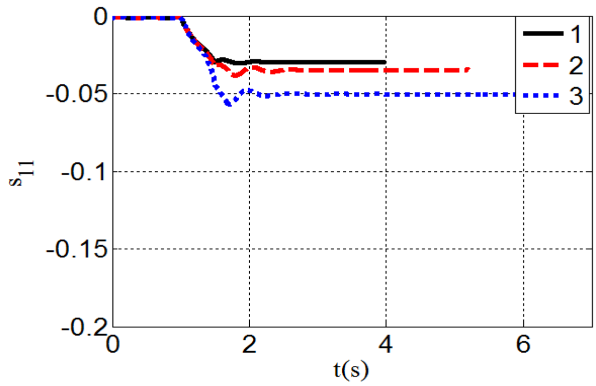

Fig. 11. Left front wheel slip coefficient. (1. Black $\varphi = 0.8$; 2. Red dashed line $\varphi = 0.7$; 3. Blue dot $\varphi = 0.5$).

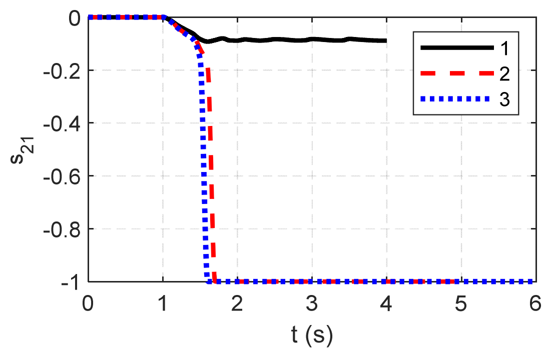

Fig. 12. Left rear wheel slip coefficient. (1. Black $\varphi = 0.8$; 2. Red dashed line $\varphi = 0.7$; 3. Blue dot $\varphi = 0.5$).

The wheel slip ratio time histories during braking on three distinct road surfaces with varying adhesion coefficients are shown in Figs. 11 and 12. The front axle wheel 11 operated inside the steady linear adhesion zone of the tire-road characteristic, as indicated by the slip ratio staying below 6% for all evaluated road conditions in Table II [29]. This result confirms that the braking force demand at wheel 11 did not exceed the available longitudinal tire force. During deceleration, longitudinal load transfer increased the normal load acting on the front axle, thereby enhancing the available tire-road adhesion and maintaining stable rolling behavior. Consequently, the braking force at wheel 11 remained lower than the maximum transmissible friction force, and no wheel lock tendency was observed. This behavior is consistent with classical vehicle braking theory, where dynamic load transfer shifts vertical force from the rear axle to the front axle during deceleration [30].

The response for the rear axle wheel 21 is noticeably different in Fig. 12. The slip ratio stayed below 10% on the high-adhesion road surface (φ = 0.8), suggesting steady tire functioning with enough traction reserve. However, on wet and lower-adhesion surfaces (φ = 0.5–0.7), the slip ratio increased rapidly and reached 100% after approximately 0.8 s of braking, indicating complete wheel lock in Table II [31]. Once wheel lock occurred, the tire transitioned from rolling adhesion to sliding friction, causing a substantial reduction in usable longitudinal force and a near loss of lateral force generation capability. This phenomenon significantly degrades directional stability and yaw controllability, particularly for rear-axle lock, which can induce vehicle oversteer, lateral instability, and tail swing. The result demonstrates that low-friction surfaces combined with dynamic rear axle unloading substantially increase the risk of rear wheel lock during severe braking [32].

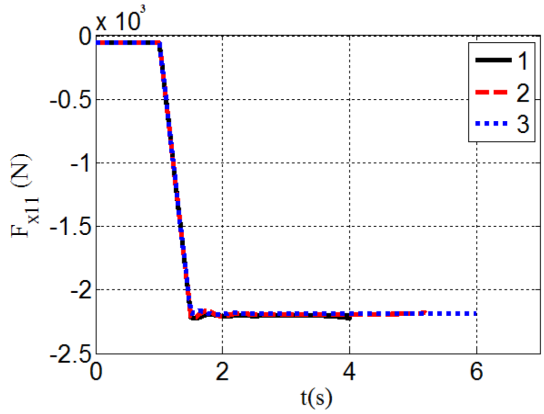

Fig. 13. Braking force at the front left wheel. (1. Black $\varphi = 0.8$; 2. Red dashed line $\varphi = 0.7$; 3. Blue dot $\varphi = 0.5$).

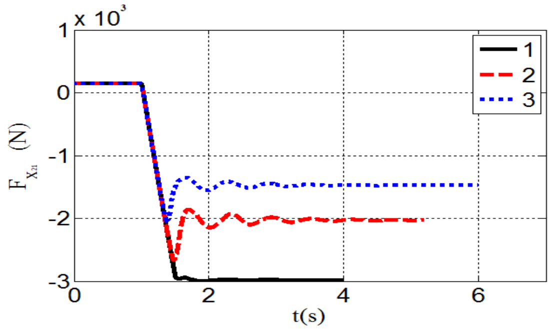

Fig. 14. Braking force at the rear left wheel. (1. Black $\varphi = 0.8$; 2. Red dashed line $\varphi = 0.7$; 3. Blue dot $\varphi = 0.5$).

Fig. 13 presents the variation of braking force during the stopping process. For all three road surfaces, the braking force at the front wheel 11 follows the same trend as the applied braking torque, indicating a direct proportional relationship between brake torque input and the generated longitudinal tire force. This confirms that, for the front axle, the available tire-road adhesion was sufficient to transmit the demanded braking force without significant saturation.

A clear quantitative difference can be observed in braking duration as the road adhesion coefficient decreases. On the dry road with high friction (φ = 0.8), the vehicle reached a complete stop in approximately 3.0 s. When the friction coefficient decreased to φ = 0.7, the braking time increased to about 4.2 s, representing an increase of nearly 40%. On the lower-adhesion surface (φ = 0.5), the stopping time further increased to approximately 4.9 s, which is about 63% longer than that on the dry road [33].

This trend can be explained by the reduction in maximum available tire-road friction force under low-adhesion conditions. Since the achievable braking force is proportional to the normal load and friction coefficient, a lower φ value limits deceleration capability, thereby extending the stopping time. These results are consistent with established braking dynamics theory and demonstrate the strong sensitivity of braking performance to road surface conditions

The maximum braking force for the rear axle wheels 21 is approximately 26 kN (corresponding to MBmax = 76% MBđm) when running on a road with a coefficient of friction $\varphi = 0.7$. The wheel slips because the braking force has surpassed the friction force threshold value, resulting in a reduction of the braking force to approximately 21kN. Fig. 14 presents that when running on a road with a coefficient of friction $\varphi = 0.5$, the maximum braking force is approximately 20 kN (corresponding to MBmax = 59% MBđm), and then it drops to approximately 15 kN [34].

According to the fundamental principles of vehicle dynamics outlined by Thomas D. Gillespie in Fundamentals of Vehicle Dynamics, the theoretical maximum deceleration achievable by a vehicle utilizing the full friction potential between the tires and the road surface is defined as $\ddot{x}_{max}$. Given a friction coefficient of $\varphi = 0.5$, this theoretical limit equals 4.905 m/s^2. Formula for determining the error between theory and experimental results:

$$Percentage\ Error = \frac{\left|\ddot{x}_{experimental} - \varphi \times g\right|}{\varphi \times g} \times 100\% \tag{13}$$

in there: φ: Adhesion coefficient; g: Gravitational acceleration.

The acceleration deviation between theory and experiment for braking acceleration with a coefficient of friction $\varphi = 0.5$ is 16.3%, $\varphi = 0.7$ is 6.7%, and $\varphi = 0.8$ is 8.2%, according to the survey results in Table III. All deviations are less than 20%, indicating that the experimental survey results are reliable and consistent with pure theory.

TABLE III. COMPARISON OF BRAKING ACCELERATION DEVIATION VALUES BETWEEN THEORY AND EXPERIMENT

Sliding Coefficient	Brake Acceleration (m/s^2)	Percentage Error (%)	Standard Brake Acceleration (m/s^2)
$\varphi = 0.5$	4.1	16.3	4.905
$\varphi = 0.7$	6.4	6.7	6.86
$\varphi = 0.8$	7.2	8.2	7.84

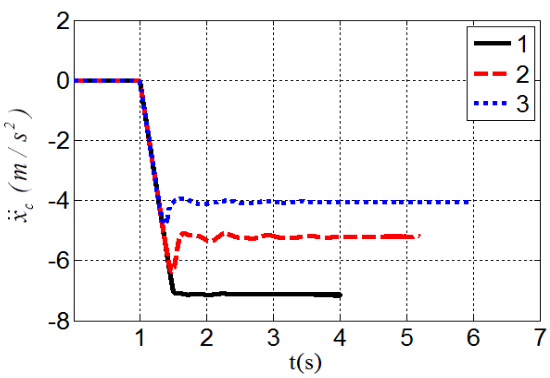

Fig. 15. Deceleration of a car during braking. (1. Black φ=0.8; 2. Red dashed line φ= 0.7; 3. Blue dot φ= 0.5).

The vehicle brake acceleration graph is displayed in Fig. 15. We see that the vehicle's braking acceleration profile is quite similar. On a good road with a coefficient of adhesion $\varphi = 0.8$, the braking duration is approximately 3 s, the braking acceleration reaches 7.2 m/s^2, and the braking efficiency is great when braking with a torque equivalent to 80% of the nominal braking torque. On a road with an average coefficient of adhesion of $\varphi = 0.7$, the braking time is approximately 4.2 s, the initial braking acceleration reaches approximately 6.4 m/s^2 after 0.5 s, and the wheels slip as a result of the braking force surpassing the adhesion threshold, causing the braking acceleration to rapidly drop to approximately 5.2 m/s^2, resulting in a 28% decrease in braking efficiency. It takes about five seconds to brake on a road with a low coefficient of friction φ =0.5). The braking acceleration reaches about 4.9 m/s² after 0.3 s of braking. Wheel slippage then causes the braking acceleration to drop sharply to about 4.1 m/s^2, which results in a roughly 43% reduction in braking efficiency [35].

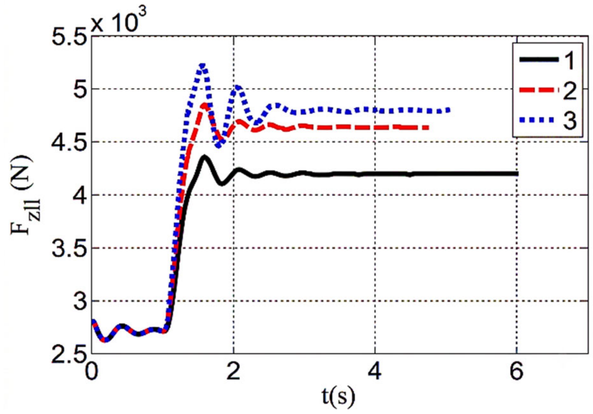

Fig. 16. Vertical reaction force at the front left wheel. (1. Black φ= 0.8; 2. Red dashed line φ= 0.7; 3. Blue dot φ= 0.5).

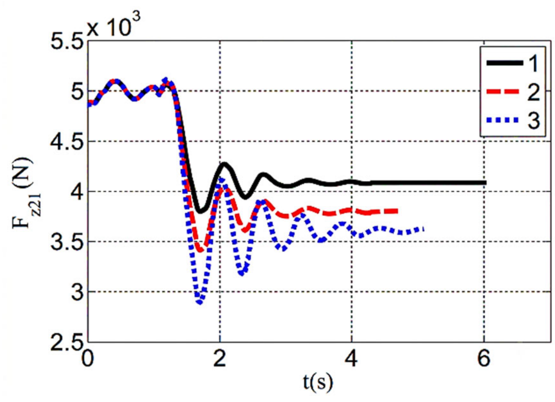

Fig. 17. Vertical reaction force at the left rear wheel. (1. Black φ= 0.8; 2. Red dashed line φ= 0.7; 3. Blue dot φ= 0.5).

The road's vertical reaction force acting on the wheels of axles 1 and 2 is shown in Figs. 16 and 17. The road's vertical response force pushing on the wheel of axle 1 rises while it falls on axle 2 during braking, as we can observe. The vertical response force of the road acting on axle 1's wheel rises when braking with a greater moment, whilst the vertical reaction force of the road acting on axles 3 and 6 falls, and vice versa. The rationale is that during braking, a longitudinal inertial force tends to push the vehicle's weight forward, transferring the load on the axles in the same direction as the motion [36].

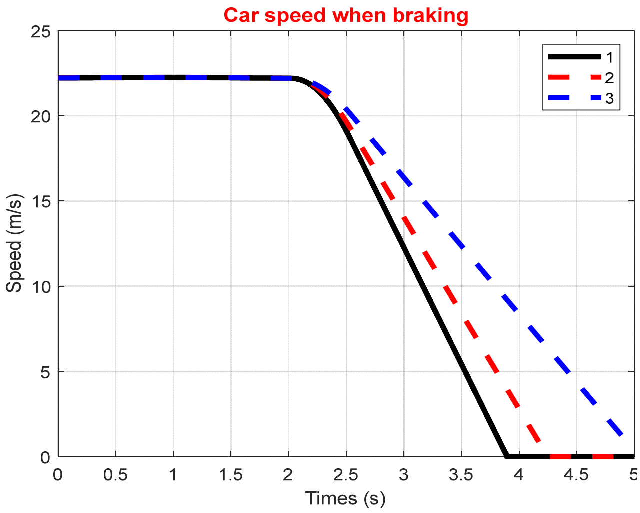

Fig. 18. The speed of the car during braking. (1. Black $\varphi = 0.8$; 2. Red dashed line $\varphi = 0.7$; 3. Blue dot $\varphi = 0.5$).

The findings of the study demonstrate that an automobile's braking characteristics are mostly determined by the coefficient of friction between the tire and the road surface. The vehicle often has a higher deceleration rate when the coefficient of friction reaches a high value (φ = 0.8), which results in noticeably shorter stopping times and distances. Fig. 18 presents that braking efficiency drastically drop when the coefficient of friction drops to $\varphi = 0.7$ and $\varphi = 0.5$, as shown by longer stopping times and slower deceleration. Wheel slippage is more likely when the coefficient of friction decreases because it restricts the amount of braking force that is transferred to the road surface [37]. This has a direct impact on the longitudinal stability of the vehicle. This outcome validates the significance of road surface conditions and the need for sophisticated braking and stability control systems to enhance operational safety under low-traction circumstances.

V. Conclusion

The experimental results clearly demonstrate that the tire-road friction coefficient strongly governs both braking performance and vehicle dynamic stability. Under high-adhesion conditions (φ = 0.8), the slip ratios of both front and rear wheels remained predominantly within the linear adhesion region, where tire forces increase proportionally with slip. In this operating range, the tires are able to transmit braking forces efficiently, resulting in stable deceleration and shorter stopping times. In addition, longitudinal load transfer during braking increases the normal force acting on the front axle, thereby enhancing front-wheel traction capacity and reducing the likelihood of premature front-wheel lock.

In contrast, under medium- and low-adhesion road conditions (φ = 0.7 and φ = 0.5), the rear axle wheels exhibited a rapid rise in slip ratio followed by early wheel lock. This indicates a transition from the adhesion region to full sliding friction, where the available longitudinal tire force decreases significantly. As a consequence, braking effectiveness deteriorated substantially, with stopping performance reduced by approximately 28% at $\varphi = 0.7$ and up to 43% at $\varphi = 0.5$ compared with the dry-road condition. The corresponding increase in braking time and decrease in achievable deceleration confirm the strong dependence of braking efficiency on surface friction.

Furthermore, the reduction in rear axle braking force—approaching 50% lower on low-friction roads than on dry pavement—adversely affects both longitudinal and lateral stability. Since locked rear wheels generate little lateral guidance force, the vehicle becomes more susceptible to yaw instability, tail swing, and loss of directional control during severe braking maneuvers. These findings emphasize the necessity of effective brake-force distribution and slip control strategies when operating on low-adhesion surfaces

Overall, the results show that reducing road adhesion raises the likelihood of wheel lock, skidding, and vehicle instability in addition to reducing braking force and acceleration. These findings demonstrate how road surface characteristics have a significant impact on braking dynamics and emphasize the need for sophisticated braking and stability control systems to guarantee safe vehicle operation in lowtraction situations.

Conflict of Interest

The authors declare no conflict of interest.

Author Contributions

P.K.T.: Conceptualization, Data curation, Formal analysis, investigation, Methodology. D.N.T. Project administration, Software, Supervision, Validation, Writing—original draft, Writing—review & editing. All authors had approved the final version.

Acknowledgment

The authors sincerely thank the invaluable support of the Faculty of Automotive Engineering Technology and Vinh Long University of Technology and Education, Vinh Long, Vietnam, in completing this research.

References

[1] M. Nassar, K. Polat, Y. Koçlu, and M. M. Topaç, "Design and optimisation of a double wishbone independent suspension system for an L6 electric vehicle: A response surface methodology based

design application," *Engineering Perspective*, vol. 4, no. 1, pp. 21–30, 2025. doi: 10.29228/eng.pers.79569

[2] R. Rajamani, *Vehicle Dynamics and Control*, 2nd ed. New York, NY, USA: Springer, 2012.

[3] D. Gürses, "Optimal design of automobile suspension control arm using metaheuristic algorithms," *International Journal of Automotive Science and Technology (IJASTECH)*, vol. 9, no. 3, pp. 305–309, 2025. doi: 10.30939/ijastech.1749077

[4] B. Baráth, "The effect of poor road surfaces on vehicle suspension geometry and the misalignment of setup parameters," *International Journal of Automotive Science and Technology (IJASTECH)*, vol. 9, 1st Future of Vehicles Conf., pp. 28–34, 2025. doi: 10.30939/ijastech.1766086

[5] D. L. Luu, N. Q. Trung, and N. T. To, "Enhancement of ride comfort in active quarter-car suspension systems using model predictive control," *International Journal of Automotive Science and Technology (IJASTECH)*, vol. 9, no. 4, pp. 527–535, 2025. doi: 10.30939/ijastech.1701968

[6] I. M. Zulhilmi, M. H. Peeie, S. M. Asyraf, I. M. Sollehudin, and I. M. Ishak, "Experimental study on the effect of emergency braking without anti-lock braking system to vehicle dynamics behaviour," *International Journal of Automotive and Mechanical Engineering*, vol. 17, no. 2, pp. 7832–7841, 2020. doi: 10.15282/ijame.17.2.2020.02.0583

[7] I. M. Zulhilmi, M. H. Peeie, R. I. M. Eiman, I. M. Izhar, and S. M. Asyraf, "Investigation on vehicle dynamic behaviour during emergency braking at different speed," *International Journal of Automotive and Mechanical Engineering*, vol. 16, no. 1, pp. 6161–6172, 2019. doi: 10.15282/ijame.16.1.2019.6.0468

[8] P. Eze, D. O. Njoku, O. C. Nwokonkwo, C. G. Onukwugha, J. N. Odii, and J. E. Jibiri, "Wheel slip equilibrium point model reference adaptive control based pid controller for antilock braking system: A new approach," *International Journal of Automotive and Mechanical Engineering*, vol. 21, no. 3, pp. 11581–11595, 2024. doi: 10.15282/ijame.21.3.2024.10.0893

[9] S. I. Haris, F. Ahmad, M. H. Che Hassan, A. K. M. Yamin, and N. R. M. Nuri, "Self tuning PID control of antilock braking system using electronic wedge brake," *International Journal of Automotive and Mechanical Engineering*, vol. 18, no. 4, pp. 9333–9348, 2021. doi: 10.15282/ijame.18.4.2021.15.0718

[10] M.-C. Wu and M.-C. Shih, "Simulated and experimental study of hydraulic anti-lock braking system using sliding-mode PWM control," *Mechatronics*, vol. 13, no. 4, pp. 331–351, 2003. doi: 10.1016/S0957-4158(01)00049-6

[11] P. M. Heerwan, M. A. Shahrom, M. I. Ishak, H. Kato, and T. Narita, "Investigation of the performance of plugging braking system as a hill descent control (HDC) for electric-powered wheelchair," *International Journal of Automotive and Mechanical Engineering*, vol. 20, no. 4, pp. 10906–10916, 2023. doi: 10.15282/ijame.20.4.2023.08.0843

[12] National Technical Standards on Technical Safety and Environmental Protection for Automobiles, QCVN Standard 09:2015/BGTVT, 2015.

[13] V. Q. Le, J. Zhang, X. Liu, and Y. Wang, "Nonlinear dynamic analysis of interaction between vehicle and road surfaces for 5-axle heavy truck," *Journal of Southeast University*, vol. 27, no. 4, pp. 405–409, 2011.

[14] A. Soltani, S. Azadi, and R. N. Jazar, "Integrated control of braking and steering systems to improve vehicle stability based on optimal wheel slip ratio estimation," *Journal of the Brazilian Society of Mechanical Sciences and Engineering*, vol. 44, 102, 2022. doi: 10.1007/s40430-022-03420-2

[15] R. N. Jazar, *Vehicle Dynamics: Theory and Application*. Cham, Switzerland: Springer Nature, 2025.

[16] V. V. Luong, T. Q. Nguyen, H. Q. Le *et al.*, "Determination of dynamic loads from the road surface acting on the chassis by experimental methods," in *Proc. IOP Conf. Ser.: Mater. Sci. Eng.*, vol. 886, no. 1, 012008, 2020. doi: 10.1088/1757-899X/886/1/012008

[17] B. Baráth, "The effect of poor road surfaces on vehicle suspension geometry and the misalignment of setup parameters," *International Journal of Automotive Science and Technology*, vol. 9, pp. 28–34, 2025. doi: 10.30939/ijastech..1766086

[18] N. Ikhsan, A. Saifizul, and R. Ramli, "The effect of vehicle and road conditions on rollover of commercial heavy vehicles during cornering: A simulation approach," *Sustainability*, vol. 13, no. 11, 6337, 2021. doi: 10.3390/su13116337

[19] T. H. Ta, V. H. Vo, and N. K. Duong, "Study on the dynamic rollover indicators of tractor semi-trailer vehicle while turning maneuvers based on multibody system dynamics analysis and newton-euler equations," in *Proc. International Conference on Advanced Mechanical Engineering, Automation, and Sustainable Development 2021 (AMAS2021)*, 2022, pp. 30–38. doi: 10.1007/978-3-030-99666-6_5

[20] Z. Ye, W. Xie, Y. Yin *et al.*, "Dynamic Rollover Prediction of Heavy Vehicles Considering Critical Frequency," *Automotive Innovation*, vol. 3, no. 2, pp. 158–168, 2020. doi: 10.1007/s42154-020-00099-w

[21] B. Zhang, C. Zong, G. Chen *et al.*, "A novel integrated stability control based on differential braking and active steering for four-axle trucks," *Chinese Journal of Mechanical Engineering*, vol. 32, no. 1, 12, 2019. doi: 10.1186/s10033-019-0323-0

[22] Z. Wang and C. Cong, "On optimizing steering performance of multi-axle vehicle based on driving force control," in *Proc. MATEC Web Conferences*, 2017, vol. 124, 07005. doi: 10.1051/matecconf/201712407005

[23] M. Topaç, O. Çolak, L. Bilal *et al.*, "Structural Analysis of a Multi-axle Steering Linkage for an 8 × 8 Special Purpose Vehicle," in *Vehicle and Automotive Engineering*, Cham: Springer, 2020. doi: 10.1007/978-981-15-9529-5

[24] G. Qin, Y. Sun, Y. Zhang *et al.*, "Analysis and optimization of the double-axle steering mechanism with dynamic loads," *The Open Mechanical Engineering Journal*, vol. 5, no. 1, pp. 26–39, 2012. doi: 10.2174/1874155X01206010026

[25] Q. Guo, D. Zhao, X. Zhao *et al.*, "Active suspension control strategy of multi-axle emergency rescue vehicle based on inertial measurement unit," *Sensors*, vol. 21, no. 20, 6877, 2021. doi: 10.3390/s21206877

[26] M. Yang, X. H. Gao, X. J. Zhang *et al.*, "Simulation analysis of multi-axle vehicle's turning braking stability based on fuzzy control theory," in *Proc. 2nd International Conference on Industrial Mechatronics and Automation*, Wuhan, China, 2010, pp. 374–377. doi: 10.1109/ICINDMA.2010.5538128

[27] S. Zhang, Y. Liu, P. Li *et al.*, "Study of instability mechanisms of trucks turning right at long downhill T-junctions based on Trucksim simulation," *PLOS ONE*, vol. 18, no. 3, e0282779, 2023. doi: 10.1371/journal.pone.0282779

[28] K. Lundahl, C. Lee, E. Frisk *et al.*, "Analyzing rollover indices for critical truck maneuvers," *SAE International Journal of Commercial Vehicles*, vol. 8, no. 1, pp. 189–196, 2015. doi: 10.4271/2015-01-1595

[29] H. B. Pacejka, *Tire and Vehicle Dynamics*, 3rd ed. Oxford, UK: Butterworth-Heinemann, 2012.

[30] X. Dong, Y. Jiang, Z. Zhong, and W. Zeng, "Rollover threshold investigation of a heavy-duty vehicle during cornering based on multi-body dynamics," *Advances in Mechanical Engineering*, vol. 10, no. 7, 2018. doi: 10.1177/1687814018789505

[31] L. Q. Jin and X. S. Chuan, "A parameterized simulation model for multi-axle vehicle," *Advanced Materials Research*, vol. 186, pp. 170–175, 2011. doi: 10.4028/www.scientific.net/amr.186.170

[32] B. Adam, J. Bengt, and S. Simone, "High speed driving stability of road vehicles under crosswinds: An aerodynamic and vehicle dynamic parametric sensitivity analysis," *Vehicle System Dynamics*, vol. 60, no. 7, pp. 2334–2357, 2022. doi: 10.1080/00423114.2021.1903516

[33] Y. H. Shen, Y. Gao, and T. Xu, "Multi-axle vehicle dynamics stability control algorithm with all independent drive wheel," *International Journal of Automotive Technology*, vol. 17, no. 5, pp. 795–805, 2016. doi: 10.1007/s12239-016-0078-x

[34] Y. Zhang, A. Khajepour, and Y. Huang, "Multiaxle/articulated bus dynamics modeling: A reconfigurable approach," *Vehicle System Dynamics*, vol. 56, no. 9, pp. 1315–1343, 2018. doi: 10.1080/00423114.2017.1420205

[35] R. Piłatowicz and W. Luty, "Modelling of dynamics of the suspension of tandem axles of a multiaxle vehicle provided with a novel load-equalising system," *IOP Conference Series: Materials Science and Engineering*, vol. 1247, no. 1, 012019, 2022. doi: 10.1088/1757-899X/1247/1/012019

[36] Z. Jin, J. Li, Y. Huang *et al.*, "Study on rollover index and stability for a triaxle bus," *Chinese Journal of Mechanical Engineering*, vol. 32, no. 1, 64, 2019. doi: 10.1186/s10033-019-0376-0

[37] Y. Chen, F. Yu, X. Li *et al.,* "Research and optimization of vehicle handling stability based on multi-body dynamics," *IOP Conference Series: Materials Science and Engineering*, vol. 688, no. 3, 033009, 2019. doi: 10.1088/1757-899X/688/3/033009

[38] A. Nicolini, F. Mocera, and A. Somà, "Multibody simulation of a tracked vehicle with deformable ground contact model," in *Proc. the Institution of Mechanical Engineers, Part K: Journal of Multi-body Dynamics*, vol. 233, no. 1, pp. 152–162, 2019. doi: 10.1177/1464419318784293